Thermodynamics and Mechanism of Protonated Cysteine Decomposition:

A Guided Ion Beam and Computational Study

P. B. Armentrout* and E. M. S. Stennett[a]

Department of Chemistry, University of Utah, Salt Lake City, Utah 84112

Abstract. A quantitative molecular description of the decomposition of protonated cysteine, H^+Cys, is provided by studying the kinetic energy dependence of threshold collision-induced dissociation (CID) with Xe using a guided ion beam tandem mass spectrometer (GIBMS). Primary dissociation channels are deamidation (yielding both NH_3 loss and NH_4^+ formation) and $(H_2O + CO)$ loss reactions, followed by an additional six subsequent decompositions. Analysis of the kinetic energy-dependent CID cross sections provides the 0 K barriers for six different reactions after accounting for unimolecular decay rates, internal energy of reactant ions, multiple ion-molecule collisions, and competition among the decay channels. To identify the mechanisms associated with these reactions, quantum chemical calculations performed at the B3LYP/6-311+G(d,p) level were used to locate the transition states (TSs) and intermediates for these processes. Single point energies of the reactants, products, and key optimized TSs and intermediates are calculated at B3LYP, B3P86, and MP2(full) levels using a 6-311+G(2d,2p) basis set. The computational characterization of the elementary steps of these reactions including the structures of the final products is validated by quantitative agreement with the experimental energetics. In agreement with previous work, deamidation is facilitated by anchimeric assistance of the thio group, which also leads to an interesting rearrangement of the intact amino acid identified computationally.

Keywords: anchimeric assistance, collision-induced dissociation, deamidation, potential energy surface, thermodynamics

Running title: Protonated Cysteine Decomposition

[a] Present address: Department of Chemistry and Biochemistry and The Biodesign Institute, Arizona State University, Tempe AZ

Introduction

The use of mass spectrometric methods to sequence peptides and proteins is a powerful analytical tool. Despite the success of such procedures, these methods often do not sequence entire proteins despite the fact that many peaks in the mass spectrum go unused, i.e., information is available that does not lead easily to sequence information. Hence, more robust models and bioinformatic tools for utilizing such data are still needed and actively being pursued [1]. In terms of *de novo* methods, it would be useful to have molecular models incorporating detailed energetic and mechanistic information for how proteins and peptides fragment, including low energy pathways that are not simple peptide bond cleavages, such as the "pathways in competition" approach [2]. Although much progress has been made from the computational side, detailed experimental information concerning such fragmentations is still in its infancy, with notable contributions on protonated systems from Klassen and Kebarle [3], Williams and coworkers [4], Laskin, Denisov, and Futrell [5], and Siu and coworkers [6,7]. The lack of quantitative information suggests that detailed studies of small peptides and even single amino acids would be valuable, hence recent work from our group has examined protonated glycine [8], asparagine [9], and diglycine [10,11].

In the present work, we comprehensively characterize the fragmentation reactions of H^+Cys formed by electrospray ionization (ESI) using gas-phase threshold collision-induced dissociation (TCID) experiments carried out in a guided ion beam tandem mass spectrometer (GIBMS). Our experimental results are compared to previous energy-resolved CID studies of Harrison and coworkers (ions formed by fast atom bombardment) [12], O'Hair, Styles, and Reid (OSR, ions formed by ESI) [13], and Rogalewicz, Hoppilliard, and Ohanessian (RHO, ions formed by ESI) [14], which are in qualitative agreement with the present study with a few notable exceptions. We complement our experimental work by examining the potential energy surfaces for all observed decompositions using theory at the B3LYP/6-311+G(d,p) level followed by single point calculations using B3LYP, B3P86, and MP2(full) levels with the 6-311+G(2d,2p) basis set. These computations build on similar work by OSR and RHO and yield

detailed step-by-step pathways for all decompositions. For the two primary dissociation channels, deamidation and (CO + H$_2$O) loss, our theoretical results generally match those of OSR at the MP2(FC)/6-31G*//HF/6-31G* level and RHO at the MP2(FC)/6-31G*//MP2(FC)/6-31G* level, although a more comprehensive examination of parallel pathways is conducted here. Mechanisms for subsequent decompositions are also examined here for the first time and an interesting rearrangement of the intact amino acid is identified. Importantly, quantitative agreement between the experimental and theoretical thermochemistry provides validation of the mechanisms and product structures.

Experimental and Computational

The Electronic Supplementary Material contains a detailed description of the experiment, analysis methods, and computational approach. Briefly, experiments are conducted using a guided ion beam tandem mass spectrometer (GIBMS) that has been described in detail previously [15,16]. Protonated cysteine is formed using an electrospray ionization (ESI) source [17] under conditions similar to those described previously [8-11,17-20]. Because the ions undergo multiple collisions (>10^4) with the ambient gas in the hexapole region of this source, they are assumed to have internal energies well described by a Maxwell-Boltzmann distribution of rovibrational states at 300 K, as verified in previous experiments [17-20]. Ions are extracted from the hexapole, mass selected using a magnetic momentum analyzer, decelerated to a well-defined kinetic energy, and focused into a radio frequency (rf) octopole ion guide that traps the ions radially [21,22]. The octopole passes through a static gas cell containing xenon kept at sufficiently low pressures that single collision conditions prevail. The reactant and product ions are mass analyzed using a quadrupole mass filter and are detected with a Daly detector [23]. Ion intensities as a function of collision energy are converted to absolute cross sections as described previously [15], with relative and absolute uncertainties of about ±5% and ±20%. Ion kinetic energies in the laboratory frame are converted to energies in the center-of-mass (CM) frame

using $E_{CM} = E_{lab}\, m/(m+M)$, where M and m are the masses of the ionic and neutral reactants, respectively. All energies herein are reported in the CM frame unless otherwise noted.

Threshold regions of the CID reaction cross sections are modeled using procedures developed elsewhere [24-26]. The Electronic Supplementary Material contains details of the analysis procedure, which includes explicitly accounting for internal and translational energy distributions, the effects of multiple collisions, the lifetime of the dissociating ions, as well as competition among parallel reactions in a full statistical treatment [26]. Because our models only represent products formed as the result of a single collision event, we explicitly measure the cross sections as a function of Xe pressure and extrapolate to zero pressure (rigorously single-collision conditions) [27]. In the present system, small but noticeable pressure effects were observed such that only data that had been extrapolated to zero pressure were analyzed.

Structures, vibrational frequencies, and energetics for all reactants, products, transition states, and intermediates were calculated using Gaussian 09 [28] at the 6-311+G(d,p) level [29,30]. Zero-point vibrational energy (ZPE) corrections scaled by 0.99 [31] were used to correct relative energies of various conformers determined from single point energy calculations carried out at the B3LYP, B3P86, and MP2(full) levels using the 6-311+G(2d,2p) basis set [29]. For the reaction pathway calculations detailed here, TSs were generally determined by relaxed potential energy surface scans (in which a likely reaction coordinate was systematically varied while allowing all other degrees of freedom to freely optimize) and were confirmed by the character of the potential energy surface scans and examination of the imaginary frequency and intrinsic reaction coordinate (IRC) calculations when needed. In previous work on protonated glycine and protonated diglycine [8,10,11], these levels of theory were found to provide accurate reproduction of several relevant experimental results.

Nomenclature

The nomenclature used to identify the different structural isomers of H$^+$Cys is based on that established previously for alkali cationized glycine [32-34]. Briefly, the conformations are
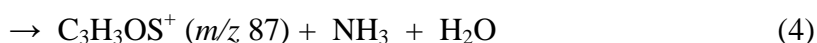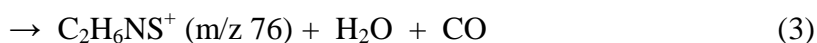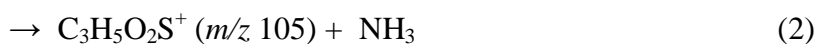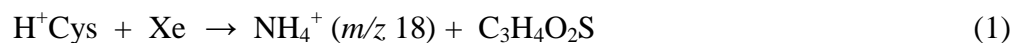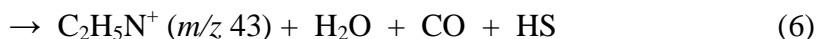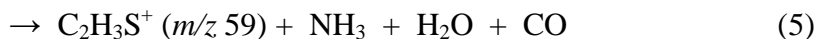
identified by their proton binding site in brackets, e.g., [N,CO,S] indicates that the proton is bound directly to the nitrogen and the NH_3^+ group forms hydrogen bonds to the carbonyl and sulfur groups. (In our previous work [35], the interaction with the sulfur side-chain was omitted because it was not needed to differentiate the four lowest energy conformers considered.) The binding site is then followed by a description of the cysteine orientation, named by the series of dihedral angles starting from the carboxylic acid hydrogen of the backbone and going to the terminal side-chain sulfur ($\angle$HOCC, $\angle$OCCC, $\angle$CCCS, and $\angle$CCSH, respectively). The dihedral angles are distinguished as cis (c, for angles between 0° - 50°), gauche (g, 50° - 130°), or trans (t, 130° - 180°). The present definitions differ from the defining angles used previously [35] (45° and 135°) because they provide more distinctive names for similar conformations. In some cases, gauche angles of the $\angle$CCSH dihedral can have opposite signs leading to distinct conformations, in which case, a subscript + and — are used to distinguish them. Our scheme for naming transition states along the calculated potential energy surfaces are specified below, but also remain a bit more complicated than simply numbering the various species. We believe such nomenclature allows better visualization of the transformations involved and can potentially be systematically extended to longer chains as well.

Results

Collision-induced Dissociation of H$^+$Cys

In our experiments, six main products are observed in the CID of H$^+$Cys at *m/z* 18, 43, 59, 76, 87, and 105, as shown in Figure 1. According to the work of O'Hair, Styles, and Reid (OSR) [13], these masses can be identified according to reactions 1 − 6, in order of their appearance energies.

$$H^+Cys + Xe \rightarrow NH_4^+ \ (m/z \ 18) + C_3H_4O_2S \qquad (1)$$

$$\rightarrow C_3H_5O_2S^+ \ (m/z \ 105) + NH_3 \qquad (2)$$

$$\rightarrow C_2H_6NS^+ \ (m/z \ 76) + H_2O + CO \qquad (3)$$

$$\rightarrow C_3H_3OS^+ \ (m/z \ 87) + NH_3 + H_2O \qquad (4)$$

$$\rightarrow C_2H_3S^+ \ (m/z \ 59) + NH_3 + H_2O + CO \qquad (5)$$

$$\rightarrow C_2H_5N^+ \ (m/z \ 43) + H_2O + CO + HS \qquad (6)$$

The kinetic energy dependence shows that reactions $1 - 3$ are primary reactions, whereas reactions $4 - 6$ involve subsequent decompositions of the primary products. OSR also performed MS/MS experiments to verify these subsequent decompositions. Here, we note that the m/z 105 product ion begins to decline near the onset of reaction 4, consistent with subsequent loss of water from the $C_3H_5O_2S^+$ product ion. The subsequent nature of this decomposition is demonstrated nicely by the fact that the sum of these two cross sections behaves smoothly with increasing energy (green solid line in Figure 1). Notably this summed cross section also declines at higher energies, which appears to be partly a consequence of the subsequent decomposition reaction 5 forming m/z 59. Contributions to this product ion from the m/z *76* precursor are also evident as the sum of the m/z 59, 87, and 105 cross sections (red dashed line in Figure 1) does not change smoothly at the onset for m/z 59. We note that OSR demonstrated both pathways for forming m/z 59 in their MS/MS studies.

At very high energies, we also observe three additional product ions with nominal masses of 26, 28, and 35, although these identifications could be off by as much as 1 amu as their small magnitudes made definitive assignments difficult in these low mass-resolution experiments. It seems plausible that m/z 28 is $HCNH^+$ formed by loss of thiol (CH_3SH) from the m/z 76 product ion, with m/z 26 being CN^+ or $C_2H_2^+$. The m/z 35 could be protonated hydrogen sulfide, H_3S^+, but all three assignments are tentative and not explored further in this work.

In early energy-resolved CID studies [12], Harrison and coworkers observed reaction 2 as the only process at their lowest relative collision energy of about 0.4 eV. This is followed by reaction 3, then reaction 4, and then reaction 5 as the collision energy was increased. This is consistent with the present work with the exceptions that no NH_4^+ was observed by Harrison, probably because the mass was too low for efficient collection in their apparatus, and their thresholds for the various product ions are almost 1 eV (center-of-mass) lower than the present work, an observation that indicates their ions are probably hot. In the study of OSR [13], the

ammonium ion was observed along with m/z 105 and 76 as the primary product ions, all having apparent thresholds near 1.2 eV relative energy with equal intensities below ~ 2 eV, center of mass. OSR studied both H^+Cys and d_2-H^+Cys in order to more readily identify the various products. (For comparison to the present data, it is worth noting that they inadvertently switched the labels of the m/z 89 and 107 d_2 products in their Figure 1.) The m/z 87 ion appears next in energy, followed by m/z 59, with m/z 43 having the highest appearance energy. Except for the relative intensities of the three primary products and their identical thresholds, all these observations are in accord with the present data. However, it is clear that the results of OSR are taken under multiple collision conditions as the precursor ion disappears completely at relative energies above about 3.5 eV, the m/z 76 ion is the dominant species present near 4 eV, and m/z 59 becomes the dominant ion from 5 eV to the highest relative energy examined, 7.3 eV. Note that the intensity of the three small products observed here, m/z 26, 28, and 35, would be too small to observe easily at this energy. Finally, RHO [14] observed reactions 2 – 5 but not reaction 1, with apparent *relative* onsets that match the present results. The ions in this study are clearly hot, as the absolute thresholds are well below those observed here (by > 1 eV in the center-of-mass frame). Also their product intensities decline rapidly above a relative energy of about 5 eV (where 10 eV is the maximum relative energy studied), indicating multiple collision conditions are probably present.

Theoretical Results: Structures of H^+Cys

Although conformations of protonated cysteine have been examined previously [14,35,36], it does not appear that a comprehensive evaluation of the possible structures has been published, with only eight distinct conformers previously characterized. Here, relative energies at 0 K including ZPE corrections for twenty-six conformers of H^+Cys calculated at three different levels of theory (B3LYP, B3P86, and MP2(full)) can be found in Table S1 with fifteen of these species shown in Figure S1. Table S1 includes a comparison to the six species previously found by Noguera et al. [36], which overlap with the likely precursor for the

fragmentation reactions located by OSR (which they called *N*) [13], and an additional conformer located by RHO [14]. Table S1 does not include oxygen protonated forms, some of which can be found in the potential energy surfaces below. Table S2 of the Electronic Supplementary Material tabulates the energetics of the TSs connecting the species in Table S1.

At all levels of theory, the lowest lying structures for H^+Cys have a [N,CO,S] coordination, a structure in which the protonated amine group hydrogen bonds to both the carbonyl oxygen atom (NH···OC) and the sulfur atom of the amino acid side chain (NH···S). A third hydrogen bond is also present between the hydroxyl group and the carbonyl oxygen atom. The four lowest energy structures having this bonding motif vary in the side-chain orientations: $tcgg_+$, $tgtg_-$, $tcgg_-$, and tgtt, with the latter three lying within $5 - 7$ kJ/mol of the $tcgg_+$ conformer, the ground structure at all levels of theory. The primary difference between $tcgg_+$ and $tcgg_-$ and between $tgtg_-$ and tgtt is simply whether the SH bond points in the same direction as the carboxylic acid group ($tcgg_+$ and $tgtg_-$) or the amino group ($tcgg_-$ and tgtt), Figure S1. On the basis of previously calculated 298 K free energies for these species [35], an equilibrium distribution of these [N,CO,S] conformers predicts that $82 - 86\%$ of the population lies in the $tcgg_+$ and $tgtg_-$ conformers with the remaining population in the $tcgg_-$ and tgtt conformers. This is consistent with the IRMPD spectra obtained previously [35].

Table S2 shows that the TS for the highest energy transformation among the various conformers of H^+Cys lies only 62 kJ/mol above the ground structure, which is well below the energy required for dissociation of H^+Cys. Thus, conversion from the ground state conformer to any of the other conformers in Figure S1 is energetically feasible well before dissociation occurs. In addition, our calculations find that sulfur protonated forms are either not stable minima on the potential energy surface or can be reached only through fairly complicated, high-energy ($98 - 117$ kJ/mol) TSs. As RHO calculate that loss of H_2S from such species lies at least 199 kJ/mol above ground H^+Cys[N,CO,S], this decomposition channel is not observed because it cannot compete with the much lower energy pathways for deamidation and (H_2O + CO) loss (see below).

Theoretical Results: Pathways for Elimination of NH_4^+ and NH_3

Table S3 of the Electronic Supplementary Material details the results of our calculations for deamidation, with Table 1 listing key transition states and products. This process involves four parallel pathways, A_N - D_N, two of which are shown in Figure 2. As previously outlined by OSR [13], elimination of ammonium and ammonia from protonated cysteine is facilitated by a backside attack of the thio group leading to a three-membered thiirane carboxylic acid (Tica). Similar behavior has been detailed for decomposition of lithiated cysteine, again forming the Tica species [37,38]. This backside attack can only occur from intermediates in which the NH_3^+ group does not interact with the thio group, i.e., from [N,CO] and [N,OH] structures. In their work, OSR identified [N,OH]ttgg– (which they called *N*) as the key intermediate, but in principle, any of the seven [N,CO] or [N,OH] intermediates can have this backside attack because they all have the thio group on the side of the backbone away from the amine, Figure S1. In practice, the lowest energy pathways involve [N,OH]ttgg– (path A_N) and its analogue, [N,CO]tcgg– (path B_N), because these species are stabilized by hydrogen bonding interactions between the SH and the CO or OH groups, respectively, Figure 2. Because the NH···OH and NH···OC hydrogen bonds are broken as the CN bond is broken, the TS for ammonia loss is preferentially stabilized by the SH···OC bond available from the [N,OH]ttgg– precursor compared to the SH···OH bond in the [N,CO]tcgg– precursor. Thus, TS[N,OH]ttgg–{C~N} (called *TSA* by OSR and *TS(M₁-B₃)* by RHO), where ~ indicates the bond is being broken, lies 1 – 10 kJ/mol below TS[N,CO]tcgg–{C~N}, and 112 – 125 kJ/mol (151 kJ/mol, OSR; 140 kJ/mol, RHO) above ground reactants, Tables 1 and S3. Pathways for NH_3 loss from [N,CO]tggg (path C_N) and [N,OH]tggg (path D_N), where the hydrogen on the sulfur points away from the carboxyl group, were also located, with {C~N} TSs lying only slightly higher in energy, 118 – 133 and 123 – 137 kJ/mol, respectively, above ground reactants (1 – 13 kJ/mol above path A_N). The other three possible precursors, [N,CO]tcgg+, [N,OH]ttgg+, and [N,OH]tggt, were found to readily rearrange to one of the other variants before reaching the TS for CN bond cleavage, Table S1.

Similar to the calculations of OSR, our exploration of the potential energy surface for path A_N finds that after passing through the {C~N} TSs, a complex of ammonia and Tica protonated on the sulfur is formed in which the ammonia binds to the alpha carbon (as indicated by the subscript), $H^+Tica[S](NH_{3,C\alpha})$ (called *IA* by OSR); however, at our level of theory, this collapses to $H^+Tica[S](NH_{3,C\beta})$ via a TS that lies lower in energy than the $C\alpha$ form (and the $C\beta$ form as well at the MP2 level) once zero point energies are included, Table S3. There are four conformers of $H^+Tica[S](NH_{3,C\beta})$ that are formed via the four pathways, Table S3. From their *IA* intermediate, OSR indicated that ammonia or ammonium ion could be lost, identifying TS[N,OH]ttgg–{C~N} (*TSA*) as the rate-limiting TS for loss of the ammonium ion. In contrast, we find that transfer of the ammonia to another more stable position on H^+Tica costs additional energy, Figure 2. Moving to the hydroxyl group over $TS(H^+Tica[S])(NH_{3,C\beta–HO})$ requires $10 - 16$ kJ/mol of energy above the {C~N} TSs along all four paths $A_N - D_N$, Table 1. Thus, the rate-limiting TSs for deamidation lie $122 - 151$ kJ/mol above ground reactants, Table 1. Once over these barriers, the system falls into a deep well with the most stable isomer being the (Tica-cc)$(NH_4^+{}_{CO})$ complex (where the $\angle HOCC$ and $\angle OCCS$ dihedral angles of Tica are specified) in which the hydroxyl proton has moved to the ammonia and the proton on the sulfur has transferred to the carbonyl, Figure 2. This species lies $10 - 14$ kJ/mol below the ground H^+Cys reactant, Table 1. Four alternative isomers of $(Tica)(NH_4^+)$ and two of $(H^+Tica)(NH_3)$ and two of were also located, Table S3. Most of these species can lose NH_4^+ to yield the Tica products, with tg–, tg+, and cc conformers all being possible (with relative energies of 0, $1 - 2$ and $4 - 7$ kJ/mol, respectively), Table 1 and Figure 2. The energy of the NH_4^+ + Tica-tg– product asymptote (called *T* by OSR) is $100 - 108$ kJ/mol (98 kJ/mol, OSR) above reactants and $19 - 25$ kJ/mol below the rate-limiting $TS(H^+Tica[S])(NH_{3,C\beta–HO})$.

Clearly, once the $H^+Tica(NH_3)$ complexes are formed, loss of ammonia is feasible once enough energy is available, with $H^+Tica[CO,S]$ttc being the ground conformer. The $H^+Tica[S,CO]$ttc conformer lies $5 - 12$ kJ/mol higher in energy and was the product identified by OSR (called *A*) and RHO (called *B₃*). We also located three additional conformations of H^+Tica,

Figure 2. Overall, loss of ammonia is limited by the loose TS associated with the final products, $H^+Tica[CO,S] + NH_3$, 140 – 155 kJ/mol above reactants, 13 – 26 kJ/mol above the rate-limiting TS, and 38 – 51 kJ/mol above the NH_4^+ + Tica-tg– products, Table 1.

OSR and RHO also examined alternative isomers of the $C_3H_5O_2S^+$ (*m/z* 105) product, identifying two stable alternatives: protonated 3-thio-propenoic acid (H$^+$Tpra, called *F* by OSR and B_2 by RHO), $H^+(HSCHCHCOOH)$, 12 kJ/mol above and 10 kJ/mol below H$^+$Tica, respectively, and a high energy (112 and 153 kJ/mol above H$^+$Tica) structure containing a 3-membered oxygen heterocycle (called *C* and B_1, respectively), Table S3. The latter structure is clearly too high in energy to consider further, but our own explorations of H$^+$Tpra located seven conformers (OSR mention two). In agreement with the MP2 calculations of OSR, we find H$^+$Tpra[S]tttt lies 22 kJ/mol above H$^+$Tica[CO,S] at the MP2 level (17 kJ/mol at B3P86), but is more stable by 2 kJ/mol at the B3LYP level. Furthermore, the ground H$^+$Tpra[S,CO]ttcc species is lower than H$^+$Tica at all levels of theory by 7 – 26 kJ/mol, in agreement with the results of RHO. Despite this lower energy, all H$^+$Tpra structures require a hydrogen atom (or carboxylic acid) shift between carbon centers in order to be formed from cysteine. Analogous processes calculated by RHO for H$^+$Ser lie about 240 kJ/mol above reactants, or 85 – 100 kJ/mol above the rate-limiting TSs for formation of H$^+$Tica. Thus, H$^+$Tpra is unlikely to be important in the decomposition of H$^+$Cys, especially near threshold.

Theoretical Results: Pathways for Rearrangement of H$^+$Cys

The computational work conducted here also elucidated an interesting rearrangement mechanism that could compete with the fragmentation process, but ultimately cannot be observed mass spectrometrically. After passing over the {C~N} TSs and forming the $H^+Tica[S](NH_{3,C\beta})$ intermediates, a covalent C_β-N bond can form, which synchronously shifts the thio group to C_α. The TSs for this shift relative to the $H^+Tica[S](NH_{3,C\beta})$ intermediates are low in energy, 2 – 10 kJ/mol for the ttc conformer, 1 – 6 kJ/mol for tcc, 1 – 5 kJ/mol for tct, and -0.2 – 1.6 kJ/mol for the ttt conformer. These TSs lie 0 – 10, 4 – 12, 7 – 14, and 11 – 16 kJ/mol

below the associated TS(H$^+$Tica[S])(NH$_{3,C\beta-HO}$) leading to dissociation, Table S3. In all cases, formation of the C$_\beta$-N bond yields protonated 2-mercapto-beta alanine, H$^+$MβAla, in which the thio and amine groups have switched carbon positions from H$^+$Cys. Five conformers of H$^+$MβAla can be formed with relative energies spanning 0 − 33 kJ/mol, Table S3. The lowest of these is shown in Figure 2 and lies 3 − 5 kJ/mol above ground H$^+$Cys.

Theoretical Results: Pathways for Elimination of NH$_3$ + H$_2$O

The H$^+$Tica (*m/z* 105) product ion can undergo further decomposition by loss of water, as shown in Figure 3, with energies summarized in Table S4 and key species in Table 2. More details of the rearrangements involved can be found in the Electronic Supplementary Material. The ground conformer of this product, H$^+$Tica[CO,S]ttc, must first rearrange to H$^+$Tica[S,CO]ttc, from which the carboxylic acid group can then rotate (in either direction) to form H$^+$Tica[S,OH]tcc, lying 19 − 27 kJ/mol above the ground conformer of this product. Now the proton on the sulfur is transferred to the hydroxyl group, which induces cleavage of the C-OH bond and forms a c-C$_3$H$_3$OS$^+$(H$_2$O) complex, Figure 3. Loss of water from c-C$_3$H$_3$OS$^+$(H$_2$O) complex requires 43 − 52 kJ/mol and forms the c-C$_3$H$_3$OS$^+$ cation, a thiirane carbonyl, Figure 3. Alternative isomers of the C$_3$H$_3$OS$^+$ species were also located, Table S4. Overall, the loss of water from the H$^+$Tica product costs 105 − 142 kJ/mol, with the overall energy of the c-C$_3$H$_3$OS$^+$ + H$_2$O + NH$_3$ products being rate limiting and lying 256 − 289 kJ/mol above the H$^+$Cys ground conformer, Table 2.

Theoretical Results: Pathways for Elimination of H$_2$O + CO

The [N,OH]ttgg$_-$ structure was also identified by OSR (called *N*) as the critical intermediate needed for elimination of water and CO. The key requirement here is that a proton on the amine group be positioned to transfer to the hydroxyl group, hence, any of the [N,OH,S] or [N,OH] conformers of H$^+$Cys should be suitable. Indeed, we find that there are six parallel pathways for water elimination, all with very similar energetics (paths A$_O$ - F$_O$), Tables 3 and S5

and Figure S2 of the Electronic Supplementary Material, with path B_O being representative, Figure 4. The path identified by OSR, path D_O here, has a TS for water loss, TS[N-OH,OH-N]ttgg$_-${C~OH} (which OSR call *TSB*, 168 kJ/mol), lying at $150 - 173$ kJ/mol. (Here our nomenclature points out that the proton remains in a shared position between the N and OH groups but shifts from the nitrogen to the hydroxyl. As this shift occurs, the C-OH bond weakens and begins to break.) The lowest energy TS we found according to DFT, TS[N-OH,OH-N]ttgg$_+${C~OH} (path A_O), lies $148 - 170$ kJ/mol above reactants, only $1 - 2$ kJ/mol below the ttgg$_-$ variant. At similar energies (lowest at the MP2 level), we also find TS[N-OH,OH-N,S]ttgg$_{+/-}${C~OH} (paths B_O and C_O). In addition, [N,OH,S]tgtg$_{+/-}$ intermediates lead to TS[N-OH,OH-N,S]tgtg$_{+/-}${C~OH}, which lie slightly higher in energy at $150 - 179$ kJ/mol above ground reactants (paths E_O and F_O). All six pathways have very similar energetics differing by only $3 - 9$ kJ/mol, Tables 3 and S5 and Figure S2, and should provide viable pathways to loss of water.

Once over the {C~OH} TSs, the molecules generally form acylium ions stabilized by the presence of the water and can potentially be viewed as the oxygen protonated forms of H^+Cys. From the $C_3H_6ONS^+(H_2O)$ complexes, the C-CO bond can then be cleaved at {C~CO} transition states to form $(CO)C_2H_6NS^+(H_2O)$ lying $20 - 87$ kJ/mol above the ground reactants. Because so much energy is released after passing over the rate-limiting TSs, it seems likely that all six pathways can explore the most stable configurations available. The most stable complex found, $(OC_{HN})C_2H_6NS^+(H_2O_{HN})$, has the water and CO bound to the two hydrogens of the amine group. Because the energy of the final products, $C_2H_6NS^+ + H_2O + CO$, also lies below the rate-limiting TS, by $30 - 61$ kJ/mol (13 kJ/mol according to the calculations of OSR), Figure 4 and Table 3, both the CO and water are rapidly eliminated and products associated with loss of only CO or only H_2O are not observed. The $C_2H_6NS^+$ product ion in this case is the cysteine immonium ion having the 1-amino-2-mercapto-ethylium cation (AMEt$^+$) structure, in agreement with OSR and RHO. We found three stable conformers of AMEt$^+$, cg (called A_1 by RHO), gg$_+$ (called *B* by OSR), and gg$_-$. The cg conformer is the lowest energy because it is stabilized by an NH···S

hydrogen bond, Figure 4. OSR and RHO also examined alternative isomers of this product ion finding the thio-substituted aziridine three-membered ring nitrogen heterocycle. This species was calculated to lie 55 and 65 kJ/mol, respectively, above AMEt$^+$, and hence was not pursued theoretically in the present work. This agrees with previous theoretical work by Barone et al. [39] on the simpler $C_2H_6N^+$ species (without the thio group). They examined seven possible isomers with the 1-amino-ethylium cation being the lowest by over 34 kJ/mol at several levels of theory.

Theoretical Results: Pathways for Elimination of H_2O + CO + HS

From AMEt$^+$, loss of the HS radical occurs simply by breaking the C-S bond. The calculated potential energy surface for this process finds no barrier in excess of the energy of the products, 233 – 284 kJ/mol above AMEt$^+$-cg and 326 – 399 kJ/mol above the ground H$^+$Cys reactants, Table 3. The $C_2H_5N^+$ radical ion formed has the vinyl amine structure, $CH_2CHNH_2^+$, and is isoelectronic with the allyl radical. Alternative isomers, $CH_3NCH_2^+$, CH_3CHNH^+ (where the NH hydrogen can be cis and trans relative to the carbon backbone), and c-$C_2H_4NH^+$, are all calculated to lie >116 kJ/mol higher in energy, Table S5.

Theoretical Results: Pathways for Elimination of H_2O + CO + NH_3

The $C_2H_3S^+$ (*m/z* 59) product can be formed via two routes. Starting with the c-$C_3H_3OS^+$ (*m/z* 87) product formed by loss of NH_3 and H_2O, Figure 3, cleavage of the C-CO bond can occur, Table 2. This TS{C~CO} is rate limiting at the B3LYP and MP2(full) levels, whereas B3P86 places the energy of the products slightly higher. The isomer of $C_2H_3S^+$ formed by this route is thiirene (c-C_2H_2S) protonated on a carbon, H$^+$c-C_2H_2S[C], but protonated thio-ketene lies lower in energy, Table 2. However, rearrangements between these structures (or of the analogous precursors) require hydrogen bond shifts that are expected to lie high in energy, e.g., the 1-2 hydrogen shift connecting H$^+$c-C_2H_2S[C] with H$^+CH_2CS$[C] lies 125 – 171 kJ/mol above

the $H^+CH_2CS[C]$ product ion (463 – 537 kJ/mol above reactants), Table S4. Thus, the protonated ketene structures are unlikely to be important in this decomposition near threshold.

Alternatively, starting with the $C_2H_6NS^+$ (*m/z* 76) product, AMEt$^+$-gg$_-$, formed by loss of H_2O and CO, the hydrogen on sulfur can transfer to the nitrogen, Table S5. This leads to amino-thiirane protonated on the nitrogen, $H^+ATi[N]$. This isomer of $C_2H_6NS^+$ lies 33 – 62 kJ/mol above AMEt$^+$-gg$_-$ (155 – 192 kJ/mol above ground H^+Cys), Table S5. Cleavage of the C-N bond in $H^+ATi[N]$ through a loose TS leads to the H^+c-$C_2H_2S[C]$ + NH_3 products directly. Thus, this route to formation of these products could dominate because the TS is slightly lower than the path above (by 0 – 10 kJ/mol) and the $C_2H_6NS^+$ (*m/z* 76) precursor has a larger cross section than the $C_3H_3OS^+$ (*m/z* 87) precursor. This is consistent with the energy dependence shown in Figure 1 and the results of OSR.

Data Analysis: Independent Channel Models

The analysis of the experimental data is challenging because of the competition among the various channels and the multiple pathways available to each product. Initially, the six major products, *m/z* 18, 105, 76, 87, 59, and 43, and their total were all analyzed independently using Equation S1. All analyses are collected in Table S6 of the Electronic Supplementary Material, which also contains a more detailed description of the analyses described briefly here, and Table S7 lists the key results. Analysis of the total cross section provides accurate thermochemistry for the lowest energy channel as well as establishing the value of the parameter *n* in Equation S1, which controls the shape of the total cross section. It was found that the four TSs along the A_N - D_N pathways lead to nearly identical results, Table S6. Various assumptions concerning the rotational symmetries of products, reaction path degeneracies, and treatment of torsional modes as rotors were also considered, Table S6. The result for fitting the total cross section listed in Table S7 is an average value for all these approaches. Similar results are obtained when analyzing the cross section sum of all channels associated with deamidation, *m/z* 18, 105, and 87. For the cross section for ammonia loss, taken as the sum of *m/z* 105 and 87, loose, tight, and

switching TS models were tried, with the latter agreeing best with the theoretical results. The results in Table S7 indicate that the results for this channel are sensitive to the assumptions made with variations in the threshold that match the different assumptions. For the loss of H_2O and CO, the m/z 76 product cross section was analyzed using several plausible assumptions for pathways A_O - F_O, and different rotational symmetries, reaction degeneracies, and torsion treatments. The result for fitting this channel independently listed in Table S7 is an average of all these approaches.

The three high energy channels (m/z 87, 59, and 43) are all limited by loose PSL TSs, however, they all involve losses of multiple neutrals, which cannot be accurately modeled using the CRUNCH software presently available. To get a rough idea of the thresholds for these channels, the parameters for the loose TS leading to NH_3 loss was utilized in all cases, with results shown in Table S7. In these three cases, we believe these thresholds are reasonable choices for the true thermochemistry because these channels are limited by loose PSL TSs, which means that appreciable competitive shifts are minimized.

Data Analysis: Competitive Models

A more accurate determination of the threshold for the two primary channels is obtained by modeling the competition between them, which is handled naturally in Equation S1 by the k_f/k_{tot} term. For a physically meaningful result, this required loosening the low-frequency modes in the H_2O + CO loss TS. Various assumptions regarding the relative reaction degeneracies and treatment of torsions were again made, Table S6, but make only small changes (less than 0.06 eV) in the thresholds and the differences in the thresholds for the two channels remains at 0.20 ± 0.07 eV. Our final experimental thresholds for these two channels in Table S5 are the average of these results, with an appropriately increased uncertainty, Tables S7 and 4. Likewise, the branching between the formation of NH_4^+ (m/z 18) and loss of NH_3 (m/z 105 + 87) can be added to the competitive model with results for simultaneously fitting all three channels shown in Figure 5. Now, only the tight TS and switching TS models were able to accurately reproduce the

data. As explained in the Electronic Supplementary Material, the experimental results indicate that the loose PSL TS for NH_3 loss must lie above the tight TS limiting the threshold for NH_4^+ production, in agreement with theory and consistent with a switching TS being the most appropriate model. Our best experimental value for this channel, Tables S5 and 4, is an average of all statistical assumptions including an increased uncertainty, Table S6. Finally, we also tried to analyze the lowest four energy product channels simultaneously by using a recently devised statistical model for sequential reactions [40], but as explained in the Electronic Supplementary Material, our best threshold for $NH_3 + H_2O$ loss (*m/z* 87) is that obtained from independent analysis, Table S7 and 4.

Discussion

The experimental thresholds for six product channels are compared to the theoretical values in Table 4 and shown graphically in Figure 6. Note that for both primary channels, the calculated asymptotic energies for NH_4^+ (*m/z* 18) and $C_2H_6NS^+$ (*m/z* 76) are well below the experimental values (by $36 - 44 \pm 12$ kJ/mol and $23 - 70 \pm 9$ kJ/mol, respectively). Thus, it is clear that both channels proceed over rate-limiting tight TSs. For NH_4^+ production and ($H_2O +$ CO) loss, the theoretical values shown include the calculated range of values for paths $A_N - D_N$ and $A_O - F_O$. One can imagine that the best experimental number could either correspond to the lowest energy threshold or be more comparable to a weighted average of the various pathways. Indeed, good agreement at all three levels of theory is obtained when viewed as the latter perspective, with reasonable agreement for the former. Because the range of TS energies is narrower for the $H_2O + CO$ loss channel, the comparison with experiment here is more discerning, with B3LYP being in closest agreement to the average, MP2 being slightly low, and B3P86 is slightly high. However, for NH_4^+ formation (*m/z* 18) and NH_3 loss (*m/z* 105), MP2 and B3P86 match well and B3LYP is low. For the three high energy products, where the experimental values do not necessarily account for all variations associated with their sequential nature, MP2 reproduces the three experimental values well with B3LYP being low and B3P86

being high. Overall the mean absolute deviation (MAD) between experiment and theory (using average tight TS values) is 23, 16, and 8 kJ/mol for B3LYP, B3P86, and MP2, with variations in the values commensurate with the experimental uncertainties of about $10 - 20$ kJ/mol. The MADs increase by $1 - 2$ kJ/mol if the lowest tight TS values are used for comparison instead.

The quantitative agreement between experiment and theory confirms that the mechanistic pathways located for deamidation and $H_2O + CO$ loss, as well as the higher energy channels, are reasonable. Further, this establishes the structure of the various products, namely deamidation forms thiirane carboxylic acid (Tica) and its protonated form (the products in Figure 2), whereas $C_2H_6NS^+$ (*m/z* 76) has an 1-amino-2-mercapto-ethylium cation structure (AMEt$^+$) (the products in Figure 4). Subsequent loss of water from H$^+$Tica (*m/z* 105) leads to a thiirane carbonyl, c-$C_3H_3OS^+$, Figure 3, which can go on to lose CO forming protonated thiirene, H$^+$c-C_2H_2S. Likewise this same product is formed by ammonia loss from AMEt$^+$, which can also lose HS to yield the radical vinyl amine cation, $CH_2CHNH_2^+$.

Thus, as originally suggested by Harrison and coworkers [12] and then explored more thoroughly by O'Hair, Styles, and Reid [13], deamidation of protonated cysteine is enabled by anchimeric assistance of the thio group. Interestingly, this nucleophilic displacement can be viewed as a simple intramolecular analogue of the key steps involved in protein splicing by inteins, which often involve cysteine residues [41]. In addition, the formation of such a cyclic species appears to facilitate an interesting rearrangement of H$^+$Cys, identified here computationally. From the key intermediates formed by backside attack of the thio group at the protonated amine, formation of a C$_\beta$-N bond yields protonated 2-mercapto-beta alanine (H$^+$MβAla), in which the thio and amine groups have switched positions from H$^+$Cys. In a peptide, such an isomerization would lengthen the backbone and could lead to unusual decomposition pathways compared to the native peptide, potentially complicating the spectra observed in sequencing experiments.

Acknowledgement

References

1. Paizs, B.; Mann, M.: 23rd Sanibel Conference on Mass Spectrometry: From Fragmentation Mechanisms to Sequencing: Tandem Mass Spectrometry Based Peptide and Protein Identification. *J. Am. Soc. Mass Spectrom.* **23**, 575-576 (2012).
2. Paizs, B.; Suhai, S.: Fragmentation pathways of protonated peptides. *Mass Spectrom. Rev.* **24**, 508-548 (2005).
3. Klassen, J. S.; Kebarle, P.: Collision-induced dissociation threshold energies of protonated glycine, glycinamide, and some related small peptides and peptide amino amides. *J. Am. Chem. Soc.* **119**, 6552-6563 (1997).
4. Schnier, P. D.; Price, W. D.; Strittmatter, E. F.; Williams, E. R.: Dissociation energetics and mechanism of leucine enkephalin $(M+H)^+$ and $(2M+X)^+$ ions (X=H, Li, Na, K, and Rb) measured by blackbody infrared radiative dissociation. *J. Am. Soc. Mass Spectrom.* **8**, 771–780 (1997).
5. Laskin, J.; Denisov, E.; Futrell, J. H.: Fragmentation energetics of small peptides from multiple-collision activation and surface-induced dissociation in FT-ICR MS. *Int. J. Mass Spectrom.* **129**, 189-201 (2002).
6. El Aribi, H.; Rodriquez, C. F.; Almeida, D. R. P.; Ling, Y.; Mak, W. W.-N.; Hopkinson, A. C.; Siu, K. W. M.: Elucidation of Fragmentation Mechanisms of Protonated Peptide Ions and Their Products: A Case Study on Glycylglycylglycine Using Density Functional Theory and Threshold Collision-Induced Dissociation. *J. Am. Chem. Soc.* **125**, 9229-9236 (2003).
7. El Aribi, H.; Orlova, G.; Rodriquez, C. F.; Almeida, D. R. P.; Hopkinson, A. C.; Siu, K. W. M.: Fragmentation Mechanisms of Product Ions from Protonated Tripeptides. *J. Phys. Chem. B* **108**, 18743-18749 (2004).
8. Armentrout, P. B.; Heaton, A. L.; Ye, S. J.: Thermodynamics and Mechanisms for Decomposition of Protonated Glycine and Its Protonated Dimer. *J. Phys. Chem. A* **115**, 11144-11155 (2011).
9. Heaton, A. L.; Armentrout, P. B.: Thermodynamics and Mechanism of Protonated Asparagine Decomposition. *J. Am. Soc. Mass Spectrom.* **20**, 852-866 (2009).
10. Armentrout, P. B.; Heaton, A. L.: Thermodynamics and Mechanisms of Protonated Diglycine Decomposition: A Computational Study. *J. Am. Soc. Mass Spectrom.* **23**, 621-631 (2012).
11. Armentrout, P. B.; Heaton, A. L.: Thermodynamics and Mechanisms of Protonated Diglycine Decomposition: A Guided Ion Beam Study. *J. Am. Soc. Mass Spectrom.* **23**, 632-643 (2012).
12. Dookeran, N. N.; Yalcin, T.; Harrison, A. G.: Fragmentation Reactions of Protonated α-Amino Acids. *J. Mass Spectrometry* **31**, 500-508 (1996).
13. O'Hair, R. A. J.; Styles, M. L.; Reid, G. E.: Role of the Sulfhydryl Group on the Gas Phase Fragmentation Reactions of Protonated Cysteine and Cysteine Containing Peptides. *J. Am. Soc. Mass Spectrom.* **9**, 1275-1284 (1998).

14. Rogalewicz, F.; Hoppilliard, Y.; Ohanessian, G.: Fragmentation mechanisms of α-amino acids protonated under electrospray ionization: a collisional activation and ab initio theoretical study. *Int. J. Mass Spectrom.* **195/196**, 565-569 (2000).

15. Ervin, K. M.; Armentrout, P. B.: Translational Energy Dependence of $Ar^+ + XY \rightarrow ArX^+ + Y$ ($XY = H_2$, D_2, HD) from Thermal to 30 eV c.m. *J. Chem. Phys.* **83**, 166-189 (1985).

16. Muntean, F.; Armentrout, P. B.: Guided Ion Beam Study of Collision-Induced Dissociation Dynamics: Integral and Differential Cross Sections. *J. Chem. Phys.* **115**, 1213-1228 (2001).

17. Moision, R. M.; Armentrout, P. B.: An Electrospray Source for Thermochemical Investigation with the Guided Ion Beam Mass Spectrometer. *J. Am. Soc. Mass Spectrom.* **18**, 1124-1134 (2007).

18. Heaton, A. L.; Armentrout, P. B.: Experimental and Theoretical Studies of Potassium Cation Interactions with the Acidic Amino Acids and Their Amide Derivatives. *J. Phys. Chem. B* **112**, 12056–12065 (2008).

19. Heaton, A. L.; Moision, R. M.; Armentrout, P. B.: Experimental and Theoretical Studies of Sodium Cation Interactions with the Acidic Amino Acids and Their Amide Derivatives. *J. Phys. Chem. A* **112**, 3319-3327 (2008).

20. Ye, S. J.; Armentrout, P. B.: Absolute Thermodynamic Measurements of Alkali Metal Cation Interactions with a Simple Dipeptide and Tripeptide *J. Phys. Chem. A* **112**, 3587-3596 (2008).

21. Teloy, E.; Gerlich, D.: Integral Cross Sections for Ion-Molecule Reactions. 1. The Guided Beam Technique. *Chem. Phys.* **4**, 417-427 (1974).

22. Gerlich, D.: Inhomogeneous rf Fields: A Versatile Tool for the Study of Processes with Slow Ions. *Adv. Chem. Phys.* **82**, 1-176 (1992).

23. Daly, N. R.: Scintillation Type Mass Spectrometer Ion Detector. *Rev. Sci. Instrum.* **31**, 264-267 (1960).

24. Rodgers, M. T.; Ervin, K. M.; Armentrout, P. B.: Statistical Modeling of Collision-induced Dissociation Thresholds. *J. Chem. Phys.* **106**, 4499-4508 (1997).

25. Armentrout, P. B.; Ervin, K. M.; Rodgers, M. T.: Statistical Rate Theory and Kinetic Energy-Resolved Ion Chemistry – Theory and Applications. *J. Phys. Chem. A* **112**, 10071-10085 (2008).

26. Rodgers, M. T.; Armentrout, P. B.: Statistical modeling of competitive threshold collision-induced dissociation. *J. Chem. Phys.* **109**, 1787-1800 (1998).

27. Hales, D. A.; Lian, L.; Armentrout, P. B.: Collision-Induced Dissociation of Nb_n^+ (n = 2 - 11): Bond Energies and Dissociation Pathways. *Int. J. Mass Spectrom. Ion Processes* **102**, 269-301 (1990).

28. Frisch, M. J.; Trucks, G. W.; Schlegel, H. B.; Scuseria, G. E.; Robb, M. A.; Cheeseman, J. R.; Scalmani, G.; Barone, V.; Mennucci, B.; Petersson, G. A.; Nakatsuji, H.; Caricato, M.; Li, X.; Hratchian, H. P.; Izmaylov, A. F.; Bloino, J.; Zheng, G.; Sonnenberg, J. L.; Hada, M.; Ehara, M.; Toyota, K.; Fukuda, R.; Hasegawa, J.; Ishida, M.; Nakajima, T.; Honda, Y.; Kitao, O.; Nakai, H.; Vreven, T.; Montgomery, J., J. A. ; Peralta, J. E.; Ogliaro, F.; Bearpark, M.; Heyd, J. J.; Brothers, E.; Kudin, K. N.; Staroverov, V. N.; Kobayashi, R.; Normand, J.; Raghavachari, K.; Rendell, A.; Burant, J. C.; Millam, J. M.; Iyengar, S. S.; Tomasi, J.; Cossi, M.; Rega, N.; Millam, J. M.; Klene, M.; Knox, J. E.; Cross, J. B.; Bakken, V.; Adamo, C.; Jaramillo, J.; Gomperts, R.; Stratmann, R. E.; Yazyev, O.; Austin, A. J.; Cammi, R.; Pomelli, C.; Ochterski, J. W.; Martin, R. L.; Morokuma, K.; Zakrzewski, V. G.; Voth, G. A.; Salvador, P.; Dannenberg, J. J.; Dapprich, S.; Daniels, A. D.; Farkas, O.; Foresman, J. B.; Ortiz, J. V.; Cioslowski, J.; Fox, D. J.: Gaussian 09, Revision A.02; Gaussian Inc.; 2009.

29. McLean, A. D.; Chandler, G. S.: Contracted Gaussian basis sets for molecular calculations. I. Second row atoms, Z=11−18. *J. Chem. Phys.* **72**, 5639-5648 (1980).

30. Krishnan, R.; Binkley, J. S.; Seeger, R.; Pople, J. A.: Self-consistent molecular orbital methods. XX. A basis set for correlated wave functions. *J. Chem. Phys.* **72**, 650-654 (1980).

31. Montgomery, J. A., Jr.; Frisch, M. J.; Ochterski, J. W.; Petersson, G. A.: A complete basis set model chemistry. VI. Use of density functional geometries and frequencies. *J. Chem. Phys.* **110**, 2822 (1999).

32. Bertran, J.; Rodriguez-Santiago, L.; Sodupe, M.: The Different Nature of Bonding in Cu^+ and Cu^{2+}-Glycine. *J. Phys. Chem. B* **103**, 2310-2317 (1999).

33. Rodriguez-Santiago, L.; Sodupe, M.; Tortajada, J.: Gas-Phase Reactivity of Ni^+ with Glycine. *J. Phys. Chem. A* **105**, 5340-5347 (2001).

34. Moision, R. M.; Armentrout, P. B.: An Experimental and Theoretical Dissection of Sodium Cation/Glycine Interactions. *J. Phys. Chem. A* **106**, 10350-10362 (2002).

35. Citir, M.; Stennett, E. M. S.; Oomens, J.; Steill, J. D.; Rodgers, M. T.; Armentrout, P. B.: Infrared Multiple Photon Dissociation Spectroscopy of Cationized Cysteine: Effects of Metal Cation Size on Gas-Phase Conformation. *Int. J. Mass Spectrom.* **297**, 9-17 (2010).

36. Noguera, M.; Rodriguez-Santiago, L.; Sodupe, M.; Bertran, J.: Protonation of glycine, serine and cysteine. Conformations, proton affinities and intrinsic basicities. *J. Molec. Struct. (Theochem)* **537**, 307-318 (2001).

37. Armentrout, P. B.; Armentrout, E. I.; Clark, A. A.; Cooper, T. E.; Stennett, E. M. S.; Carl, D. R.: An Experimental and Theoretical Study of Alkali Metal Cation Interactions with Cysteine. *J. Phys. Chem. B* **114**, 3927–3937 (2010).

38. Armentrout, P. B.; Ye, S. J.; Gabriel, A.; Moision, R. M.: Energetics and Mechanism for the Deamination of Lithiated Cysteine. *J. Phys. Chem. B* **114**, 3938–3949 (2010).

39. Barone, V.; Lelj, F.; Grande, P.; Russo, N.: Structures and relative stabilities of $[C_2H_6N]^+$ ions: A non-empirical and MNDO study. *Journal of Molecular Structure: THEOCHEM* **124**, 319-324 (1985).

40. Armentrout, P. B.: Statistical modeling of sequential collision-induced dissociation. *J. Chem. Phys.* **126**, 234302 (2007).

41. Perler, F. B.: Protein Splicing Mechanisms and Applications. *IUBMB Life* **57**, 469-476 (2005).

Table 1. Relative energies (kJ/mol) of transition states (with imaginary frequencies in cm^{-1}) and intermediates for NH_3/NH_4^+ loss from H^+Cys [a]

Structure[b]	path	imag. freq	B3LYP	B3P86	MP2(full)[b]
TS[N,OH]ttgg$_-${C~N}	A_N	49	112.3	124.5	124.9
(*TSA, TS(M$_1$-B$_3$)*)					(*151, 140*)
TS[N,CO]tcgg$_-${C~N}	B_N	55	120.9	134.3	125.7
TS[N,OH]tggg{C~N}	C_N	64	118.6	132.5	125.6
TS[N,CO]tggg{C~N}	D_N	64	123.0	137.3	129.8
TS(H$^+$Tica[S]ttc)(NH$_{3,C\beta-HO}$)	**A_N**	**104**	**122.3**	**133.2**	**128.4**
TS(H$^+$Tica[S]tcc)(NH$_{3,C\beta-HO}$)	**B_N**	**116**	**132.5**	**145.7**	**139.0**
TS(H$^+$Tica[S]ttt)(NH$_{3,C\beta-HO}$)	**C_N**	**97**	**134.3**	**148.3**	**143.1**
TS(H$^+$Tica[S]tct)(NH$_{3,C\beta-HO}$)	**D_N**	**112**	**136.7**	**151.0**	**145.1**
Tica-tg$_-$ + NH$_4^+$　(*T*)			**99.9**	**108.5**	**103.3 (*98*)**
Tica-tg$_+$ + NH$_4^+$			101.9	110.4	104.9
Tica-cc + NH$_4^+$			106.9	112.7	108.7
H$^+$Tica[CO,S]ttc + NH$_3$			**139.8**	**146.7**	**154.5**
H$^+$Tica[S,CO]ttc + NH$_3$			146.2	158.4	160.0
(*A, B$_3$*)					(*189, 180*)
H$^+$Tica[S]ttt + NH$_3$			156.4	171.1	172.4
H$^+$Tica[S,OH]tcc + NH$_3$			159.3	173.8	173.9
H$^+$Tica[S]tct + NH$_3$			162.0	177.4	178.2

[a] Calculations performed at the stated level of theory using a 6-311+G(2d,2p) basis set with geometries and vibrational frequencies calculated at B3LYP/6-311+G(d,p) level. Energies include ZPE corrections scaled by 0.99 and are relative to ground H$^+$Cys[N,CO,S]tcgg$_+$. Entries in bold are product or rate-limiting TS species. Transition states either correspond to bond cleavages (e.g., {C~N}) or migrations of the ammonia from the C$_\beta$ site to the hydroxyl group.

[b] Names and values in italics are from OSR [13] and RHO [14].

Table 2. Relative energies (kJ/mol) of transition states (with imaginary frequencies in cm^{-1}) and intermediates for H_2O and CO loss from H$^+$Tica (*m/z* 105)[a]

Structure	imag. freq	B3LYP	B3P86	MP2(full)
H$^+$Tica[CO,S]ttc		139.8	146.7	154.5
c-C$_3$H$_3$OS$^+$ + H$_2$O		**256.5**	**289.2**	**260.3**
TS(c-C$_3$H$_3$OS$^+${C~CO}) + H$_2$O	256	**345.8**	392.5	**363.3**
H$^+$c-C$_2$H$_2$S$^+$[C] + CO + H$_2$O		337.3	**396.6**	353.4
H$^+$c-C$_2$H$_2$S$^+$[S] + CO + H$_2$O		366.3	425.8	388.1
H$^+$CH$_2$CS$^+$[C] + CO + H$_2$O		214.6	283.3	216.8
H$^+$CH$_2$CS$^+$[S] + CO + H$_2$O		306.3	376.6	353.9

[a] Calculations performed at the stated level of theory using a 6-311+G(2d,2p) basis set with geometries and vibrational frequencies calculated at B3LYP/6-311+G(d,p) level. Energies include ZPE corrections scaled by 0.99, include NH_3, and are relative to ground H$^+$Cys[N,CO,S] tcgg$_+$. Entries in bold are product or rate-limiting TS species. The transition state corresponds to a bond cleavage ({C~CO}).

Table 3. Relative energies (kJ/mol) of transition states (with imaginary frequencies in cm^{-1}), intermediates, and products for H_2O + CO loss from H^+Cys [a]

Structure[b]	path	imag. freq	B3LYP	B3P86	MP2(full)[b]
TS[N-OH,OH-N]ttgg$_+${C~OH}	A$_O$	77	**153.9**	**170.5**	**147.7**
TS[N-OH,OH-N,S]ttgg$_+${C~OH}	B$_O$	65	**154.2**	**174.9**	**145.8**
TS[N-OH,OH-N,S]ttgg$_-${C~OH}	C$_O$	66	**154.5**	**175.6**	**144.4**
TS[N-OH,OH-N]ttgg$_-${C~OH} (*TSB*)	D$_O$	86	**155.1**	**172.7**	**149.6 (*168*)**
TS[N-OH,OH-N,S]tgtg$_-${C~OH}	E$_O$	57	156.7	178.4	150.0
TS[N-OH,OH-N,S]tgtg$_+${C~OH}	F$_O$	52	**157.0**	**178.9**	**150.3**
TS($C_3H_6ONS^+$-tg$_-$)($H_2O_{C\text{-}HN}$)	E$_O$	47	**157.9**	**182.0**	153.0
TS($C_3H_6ONS^+$-tg$_-$)(H_2O_{HN}){C~CO}	E$_O$	24	155.4	179.5	**154.1**
AMEt$^+$-gg$_-$(H_2O_{HN}) + CO	D$_O$, F$_O$		35.0	81.8	54.4
AMEt$^+$-gg$_+$(H_2O_{HN}) + CO	E$_O$		35.3	82.4	55.4
(OC$_{HNt}$)AMEt$^+$-gg$_-$ + H_2O			76.4	124.2	95.3
(OC$_{HNc}$)AMEt$^+$-gg$_-$ + H_2O			77.8	125.4	95.2
(OC$_{HN}$)AMEt$^+$-gg$_+$ + H_2O			77.8	125.6	95.9
AMEt$^+$-cg + H_2O + CO (*A$_1$*)	**C$_O$**		**92.6**	**139.9**	**113.0 (*145*)**
AMEt$^+$-gg$_+$ + H_2O + CO (*B*)	A$_O$, B$_O$		95.9	144.7	122.5 (*165*)
	E$_O$, F$_O$				
AMEt$^+$-gg$_-$ + H_2O + CO	D$_O$		96.1	144.6	121.9
H^+c-$C_2H_2S^+$[C] + NH_3 + H_2O + CO			**337.3**	**396.6**	**353.4**
$CH_2CHNH_2^+$ + H_2O + CO + SH			**326.1**	**398.8**	**396.7**

[a] Calculations performed at the stated level of theory using a 6-311+G(2d,2p) basis set with geometries and vibrational frequencies calculated at B3LYP/6-311+G(d,p) level. Energies include ZPE corrections scaled by 0.99 and are relative to ground H^+Cys[N,CO,S]tcgg$_+$. Entries in bold are product or rate-limiting TS species. Transition states either correspond to bond cleavages (e.g., {C~OH}), or migrations of water as designated by the subscripts. [b] Names and values in italics are from OSR [13] and RHO [14].

Table 4. Experimental and theoretical reaction energies (kJ/mol) for decomposition of H^+Cys^a

Products	Exp	limiting TS	B3LYP	B3P86	MP2(full)
$18(NH_4^+) + C_3H_4O_2S$	144 (12)	$TS(H^+Tica)(NH_{3,C\beta\text{-}HO})$	122 – 137	133 – 151	128 – 145
		products	100	108	103
$105 + NH_3$	160 (12)	switch TS	140	147	155
$76 + H_2O + CO$	163 (9)	TS{C~OH}	154 – 158	170 – 182	144 – 154
		products	93	140	113
$87 + NH_3 + H_2O$	263 (15)	products	256	289	260
$59 + H_2O + CO + NH_3$	363 (22)	products	337	397	353
$43 + H_2O + CO + HS$	388 (24)	products	326	399	397
MAD^b			23 (21)	16 (12)	8 (4)

[a] Experimental values are best values from Table S7 with uncertainties in parentheses.
Theoretical values, taken from Tables 1 – 3 (bolded entries), are performed at the stated level of
theory using a 6-311+G(2d,2p) basis set with ZPE corrections scaled by 0.99 and geometries
determined at the B3LYP/6-311+G(d,p) level. [b] Mean absolute deviation from experimental
values. Mean values for the TSs are used for comparison.

Figure Captions

Figure 1. Cross sections for collision-induced dissociation of H^+Cys with Xe as a function of kinetic energy in the center-of-mass frame (lower *x*-axis) and the laboratory frame (upper *x*-axis). Primary channels are indicated by solid symbols with sequential decompositions shown by open symbols. Lines indicate the sum of product cross sections: *m/z* 105 + 87, green solid line; *m/z* 105 + 87 + 59, red dashed line;

Figure 2. Reaction coordinate surface for deamidation from H^+Cys showing two of four possible pathways, paths A_N (full line) and B_N (dashed line), along with several variants of the products for NH_4^+ formation (*m/z* 18) and NH_3 loss (*m/z* 105). Geometry optimizations and single point energies of each elementary step are determined at the B3LYP/6-311+G(d,p) level of theory and corrected for ZPE.

Figure 3. Reaction coordinate surface for subsequent loss of water from the NH_3 loss product, H^+Tica (*m/z* 105). Geometry optimizations and single point energies of each elementary step are determined at the B3LYP/6-311+G(d,p) level of theory and corrected for ZPE. Short dashed lines indicate bonds that are breaking or forming for transition states.

Figure 4. Reaction coordinate surface for loss of water and CO from H^+Cys to form $C_2H_6NS^+$ (*m/z* 76) showing one of six possible pathways (path B_O). Geometry optimizations and single point energies of each elementary step are determined at the B3LYP/6-311+G(d,p) level of theory and corrected for ZPE.

Figure 5. Symbols show data for the indicated process as a function of collision energy between H^+Cys and Xe in the center-of-mass frame (lower x-axis) and the laboratory frame (upper x-axis). Solid lines show the best fit to the data using the model of Equation 1 convoluted over the neutral and ion kinetic and internal energy distributions. Dashed lines show the model cross sections in the absence of experimental kinetic energy broadening for reactions with an internal energy of 0 K. Model shown is for H_2O + CO loss (m/z 76) over the tight transition state of path B_O competing with deamidation over the tight transition state of path A_N followed by formation of NH_4^+ (m/z 18) or loss of NH_3 (m/z 105+87) where the latter is treated using a switching transition state.

Figure 6. Comparison of experimental threshold energies with B3LYP (blue triangles), B3P86 (green inverted triangles), and MP2 (red circles) single point energies. All values taken from Table 4. Minimum and maximum computed values for the NH_4^+ and H_2O + CO loss channels are included. Note the break in scale. Diagonal line shows perfect agreement.
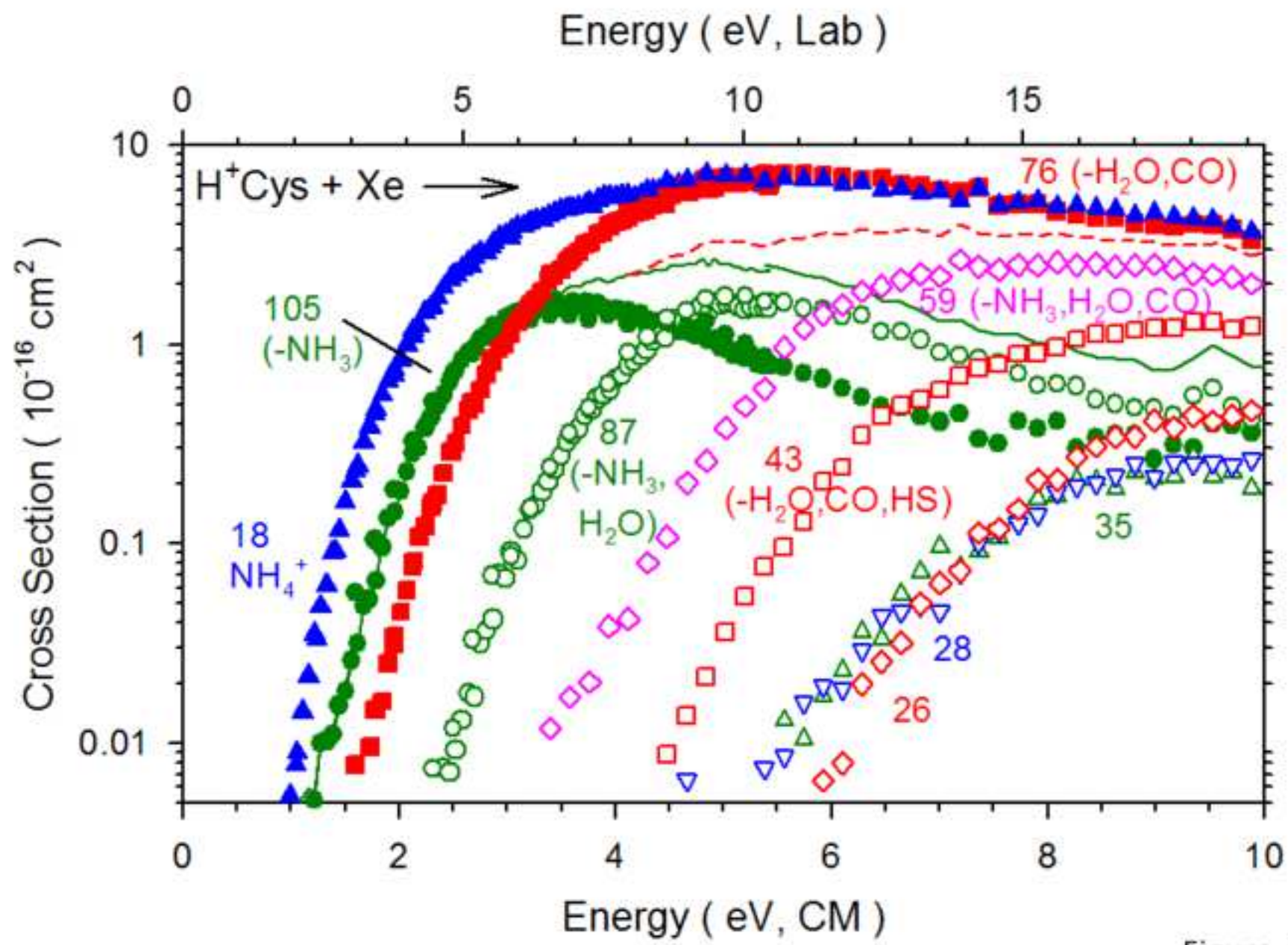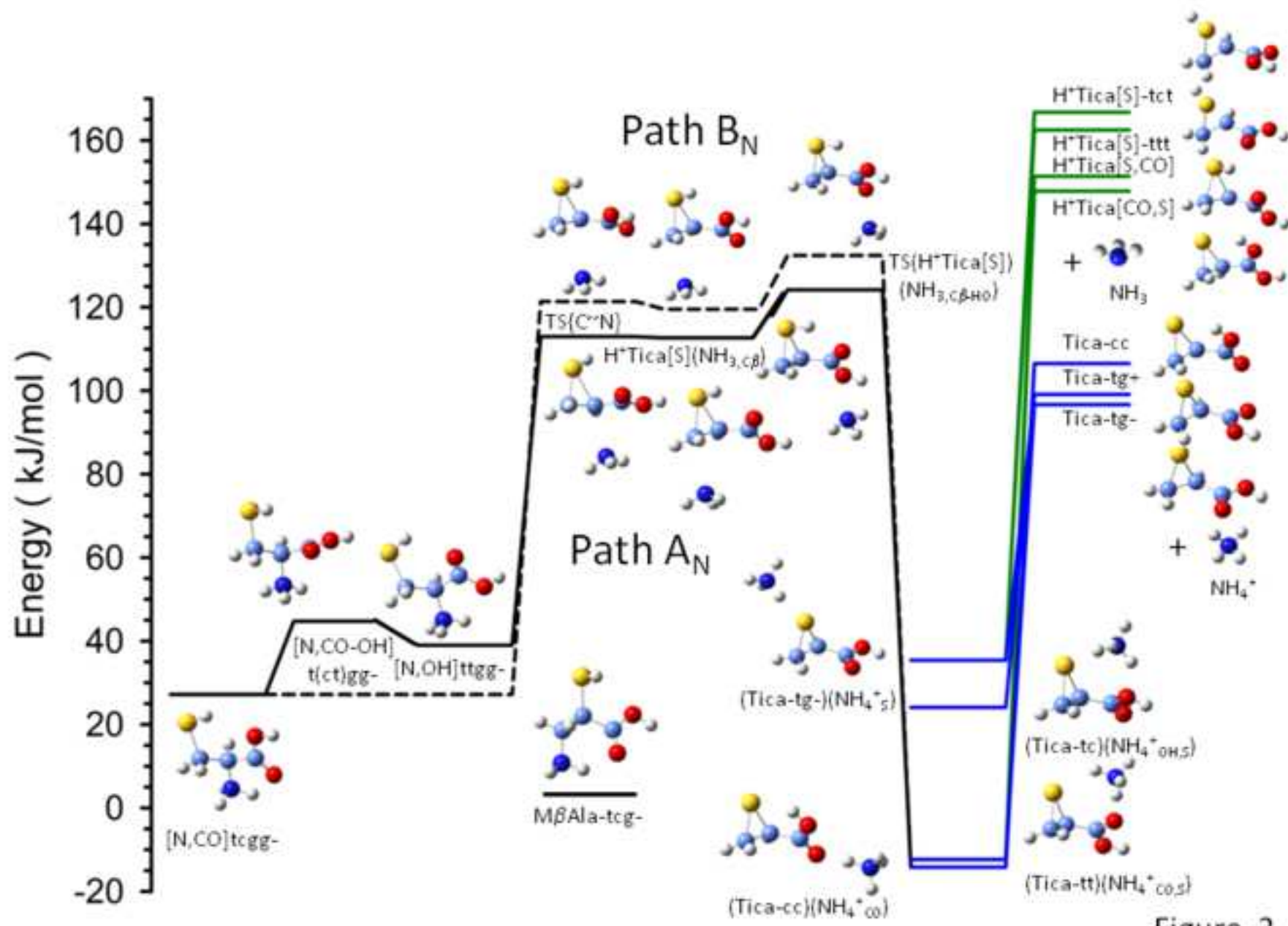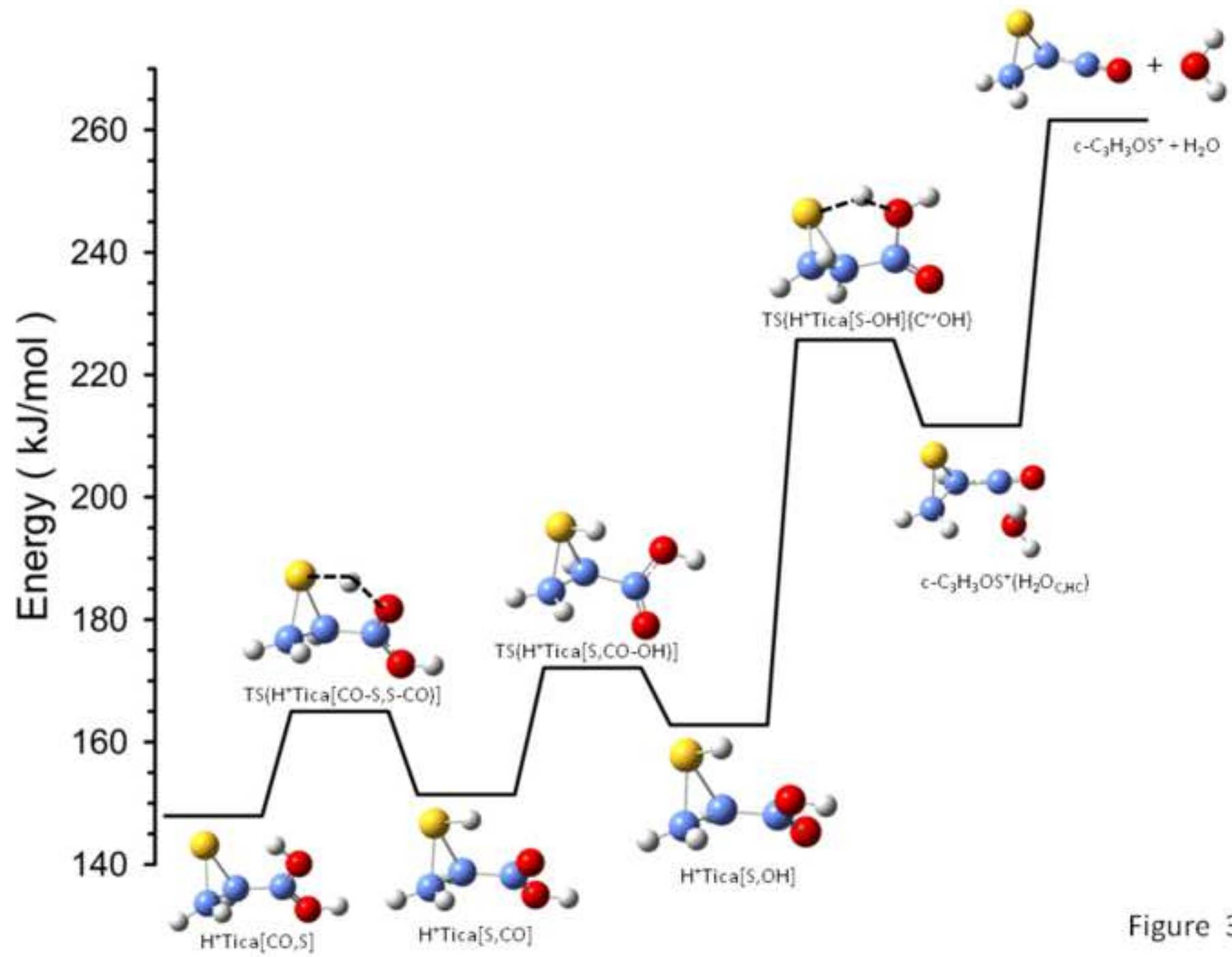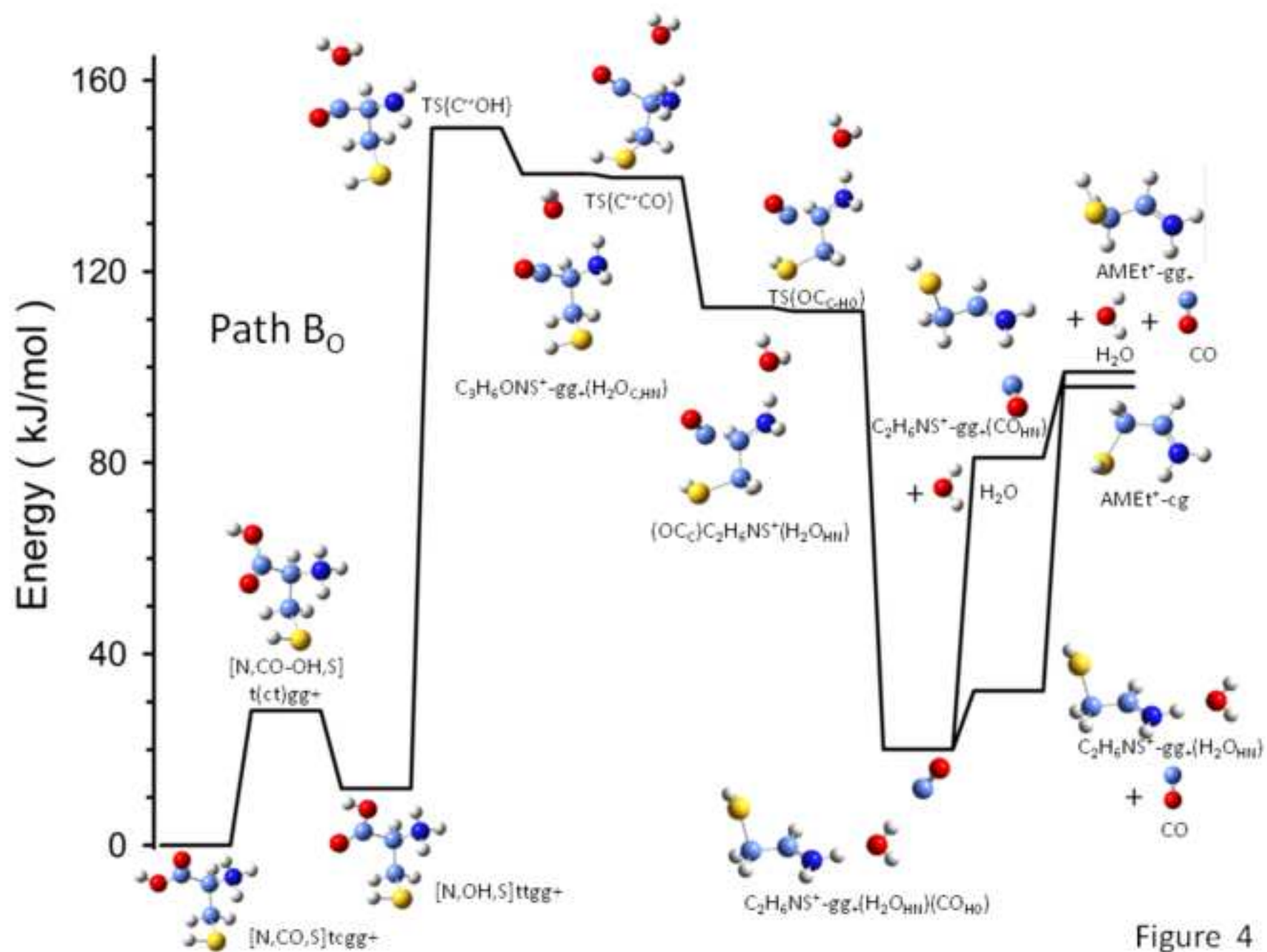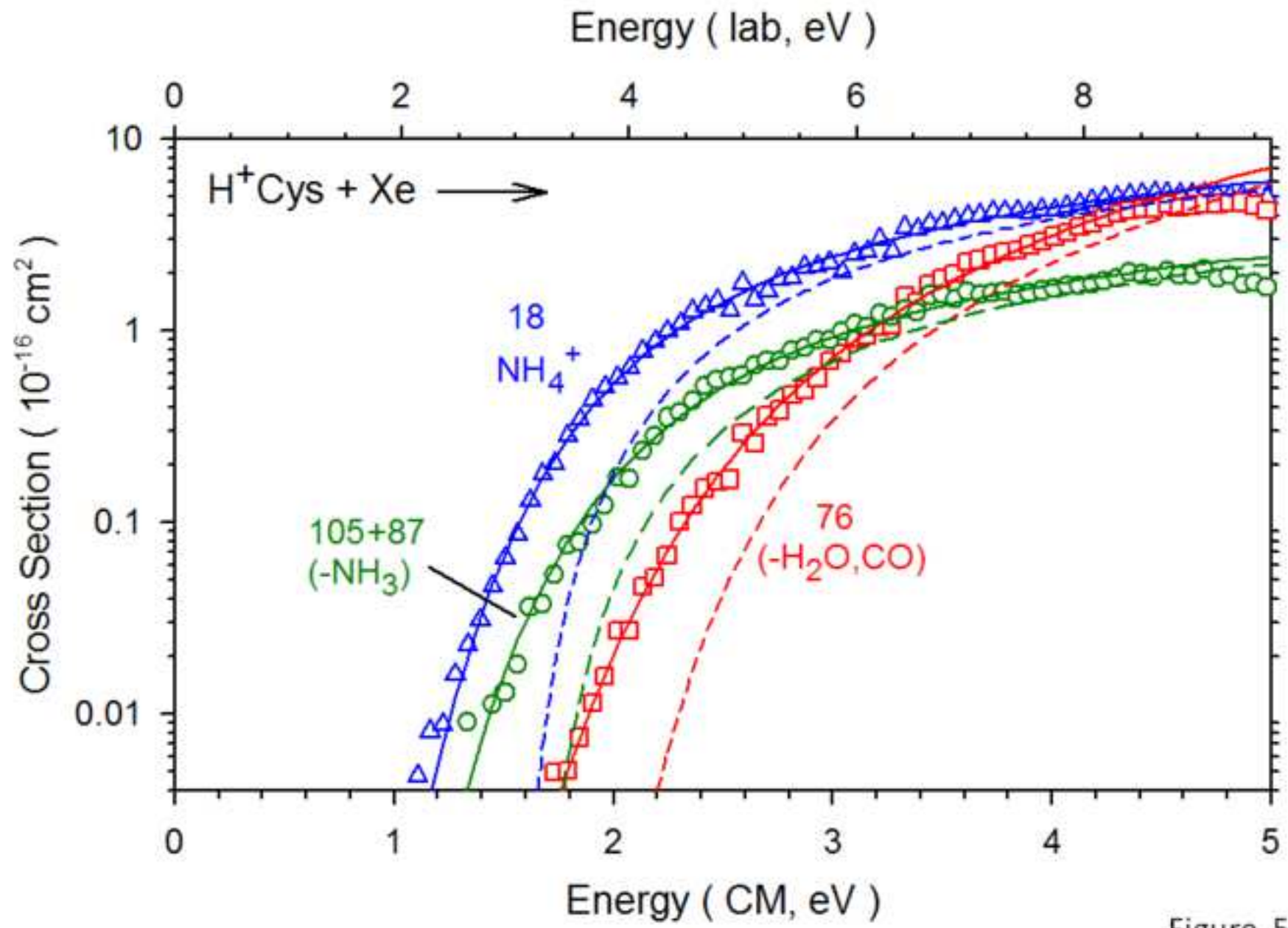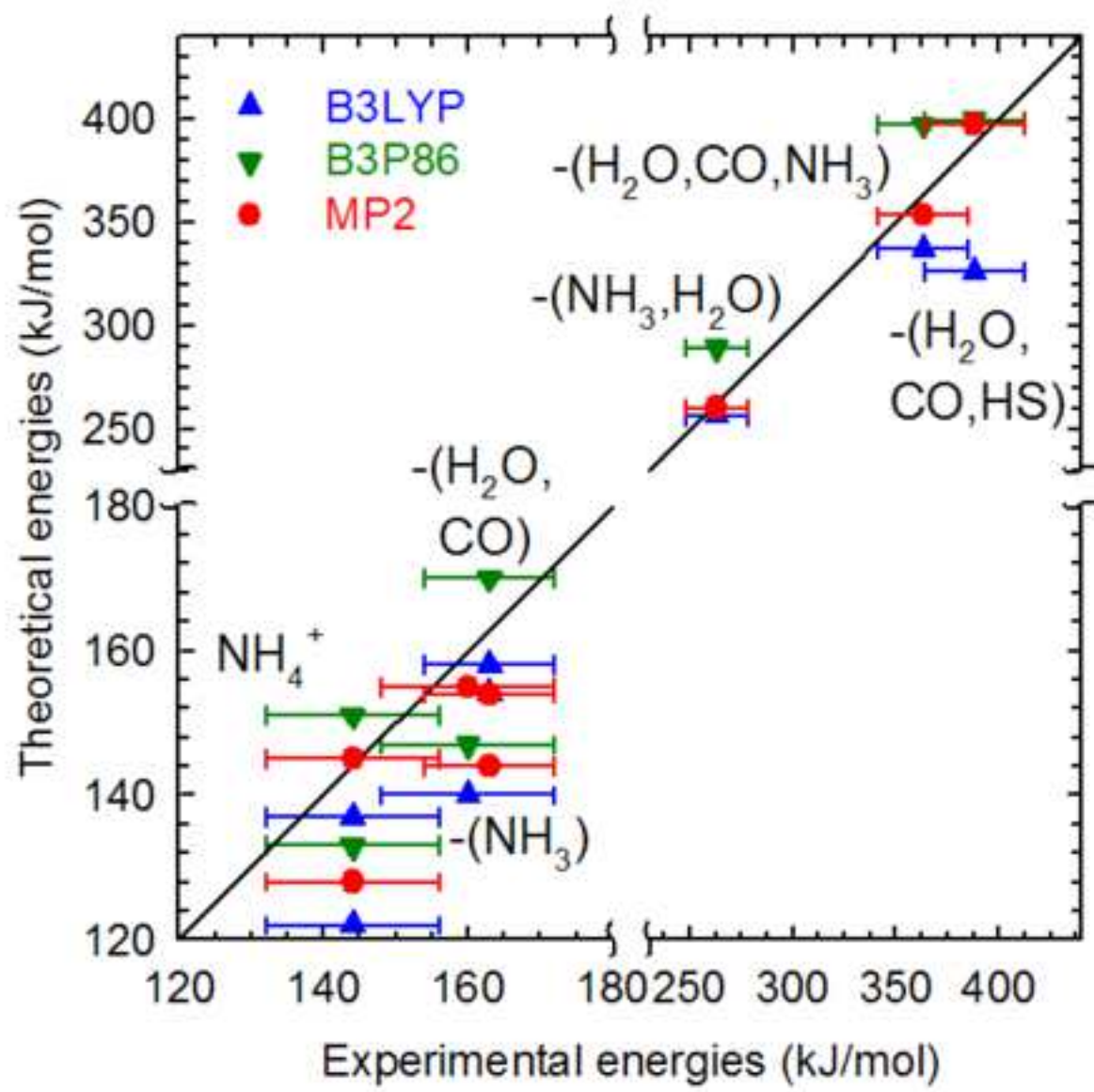
Figure 1

Figure 2

Figure 3

Figure 4

Figure 5

Figure 6